NASA TECHNICAL MEMORANDUM

NASA TM-78932

NASA TM-78932

A FLUCTUATION-INDUCED PLASMA TRANSPORT DIAGNOSTIC BASED UPON FAST-FOURIER TRANSFORM SPECTRAL ANALYSIS

by E. J. Powers, Y. C. Kim, and J. Y. Hong
The University of Texas at Austin
Austin, Texas

and

J. R. Roth and W. M. Krawczonek
Lewis Research Center
Cleveland, Ohio

TECHNICAL PAPER presented at the
International Conference on Plasma Science
sponsored by the Institute of Electrical and Electronics Engineers
Monterey, California, May 15-18, 1978

A FLUCTUATION-INDUCED PLASMA TRANSPORT DIAGNOSTIC BASED UPON FAST-FOURIER TRANSFORM SPECTRAL ANALYSIS

E. J. Powers, Y. C. Kim and J. Y. Hong
The University of Texas at Austin
Austin, Texas 78712 U.S.A.

and

J. R. Roth and W. M. Krawczonek
NASA Lewis Research Center
Cleveland, Ohio 44135 U.S.A.

E-9675

ABSTRACT

The objective of this paper is to describe a diagnostic, based on fast Fourier-transform spectral analysis techniques, that provides experimental insight into the relationship between the experimentally observable spectral characteristics of the fluctuations and the fluctuation-induced plasma transport. The key ideas underlying the approach have been described elsewhere. In this paper, we review the model upon which the diagnostic technique is based, describe its experimental implementation, and present as examples some characteristic results obtained during the course of an experimental study of fluctuation-induced transport in the electric field dominated NASA Lewis Bumpy Torus plasma.

INTRODUCTION

The theoretical principles on which this diagnostic is based have been described by Powers (1). To apply this diagnostic technique it is not necessary to have detailed knowledge of the physical processes

STAR Category 75

which give rise to the fluctuation spectra. All that is required is the capability to measure certain characteristics (described in (1)) of the density and potential fluctuation spectra. This is done by digitizing signals proportional to the density $\tilde{n}$ and potential $\tilde{\phi}$ fluctuations and computing their respective Fourier transforms using the FFT algorithm (2). From the transforms various spectral quantities are computed, the most important of which is the transport spectral density function $T(\omega)$ which indicates in a quantitative way how much transport (particles/area-time-frequency) is associated with various spectral bands. To gain further experimental insight into the factors affecting the magnitude and direction of transport, additional spectral functions are generated which indicate the frequency dependence of (1) the rms amplitudes of $\tilde{n}$ and $\tilde{\phi}$ (2) the phase angle between $\tilde{n}$ and $\tilde{\phi}$ and (3) the degree of mutual coherence (1) betwen $\tilde{n}$ and $\tilde{\phi}$.

Low frequency ($\omega << \omega_{ci}$) fluctuations are assumed such that the fluctuating particle velocity is given by $\tilde{E}xB/B^2$, where $\tilde{E}$ is the fluctuating electric field and B is the static confining magnetic field. The particle flux is given by

$$\Gamma = \langle \tilde{n}\tilde{v} \rangle = \langle \tilde{n}\tilde{E}_{\perp} \rangle / B \qquad (1)$$

To relate potential $\tilde{\phi}$ and electric field $\tilde{E}$ fluctuations, we assume a quasi-static approximation $\tilde{E} = -\nabla\tilde{\phi}$. As is shown in (1), the particle flux Γ can be expressed in terms of a transport spectral density function $T(\omega)$ as follows

$$\Gamma = \langle \tilde{n}\tilde{v} \rangle = \int_0^\infty T(\omega) d\omega \qquad (2)$$

where $T(\omega)$ is given by

$$T(\omega) = 2k(\omega) Q_{n\phi}(\omega)/B \qquad (3)$$

The quantity $Q_{n\phi}(\omega)$ is the quadrature spectrum between the density and potential fluctuations and indicates that the transport associated with any spectral band depends upon the product of the density and potential fluctuation components which are in phase quadrature. The factor $k(\omega)$ in Eq. (3) comes from the quasi-static approximation relating $\tilde{E}$ and $\tilde{\phi}$. The factor 2 in Eq. (3) takes into account the "negative frequency" contributions to the particle transport ($T(\omega)$ is an even function of frequency).

Although Eq. (3) is used to compute the transport spectra shown in this paper, additional physical insight may be obtained by noting that the transport associated with a small spectral band of width $\delta\omega$ and centered at ω may also be expressed as (1)

$$T(\omega)\delta\omega = \frac{k(\omega)}{B} n_{rms}(\omega) \phi_{rms}(\omega) \sin \alpha_{n\phi}(\omega) \, |\gamma_{n\phi}(\omega)| \qquad (4)$$

where n_{rms} and ϕ_{rms} denote the rms values of the density and potential fluctuations associated with those spectral components of bandwidth $\delta\omega$ centered at ω. The quantities $\alpha_{n\phi}(\omega)$ and $|\gamma_{n\phi}(\omega)|$ denote the phase difference and degree of mutual coherence between the density and

potential fluctuations, respectively. The appearance of the degree of mutual cohrerence $|\gamma_{n\phi}(\omega)|$ is a consequence of the polychromatic nature of the fluctuations. Further discussion of both Eqs. (3) and (4) may be found in (1).

EXPERIMENTAL IMPLEMENTATION

In order to implement the concepts reviewed in the previous section and described more fully in (1), it is necessary to develop a data acquisition system that enables one to simultaneously acquire and digitize density and potential fluctuation data, and transfer the raw time series data to a computer for processing. Since we wish to express all spectra of interest (particularly the transport spectra) in absolute physical units, it is also necessary to enter into the computer system calibration data (e.g., voltage range settings on the digitizer, preamplifier gain settings, etc.). The system used to acquire the data shown in the next section is described in detail in (4). Transient recorders were used to digitize both the density and potential fluctuation data. All the spectra included in this paper were computed from a digitized version of $\tilde{n}$ or $\tilde{\phi}$ consisting of 2048 8-bit words.

The experimental data presented in the next section was taken during the course of a study of fluctuation-induced transport in the NASA Lewis Bumpy Torus plasma (3,5). This steady-state magnetically confined toroidal plasma is acted upon by strong electric fields externally imposed along the minor radius of the plasma. It employs a modified Penning discharge to produce and heat a plasma in a bumpy toroidal

magnetic field geometry produced by 12 superconducting coils, each having an I.D. of 19 cm and capable of producing 3 Tesla on axis. The coils form a toroidal array 1.52 meters in major diameter. A steady-state plasma is created when electrodes are placed at the midplane of one or more of the twelve toroidal sectors. The electrodes can be biased with positive or negative d.c. potentials in excess of 10kV, with respect to the grounded magnet dewars. This combination of strong crossed electric and magnetic fields can produce a steady-state deuterium plasma of density 10^{8}-10^{12} cm^{-3}, ion kinetic temperatures of 340-2500 eV, and electron kinetic temperatures of 8-140 eV. Since Langmuir and capacitive probes are used to measure $\tilde{n}$ and $\tilde{\phi}$, the operating conditions had to be restricted to the low end of these ranges of kinetic temperatures in order to avoid damage to the probes.

The strong radial electric field ($\simeq$ 100v/cm) associated with the Penning discharge and the strong toroidal magnetic field give rise to a diversity of ExB phenomena such as rotating waves and spokes, which in turn manifest themselves as space-time fluctuations of the plasma density and potential. These fluctuations are monitored with an array of three probes shown schematically in Fig. 1. Fluctuations in ion density were monitored with the aid of a Langmuir probe biased into the ion saturation regime. Potential fluctuations were measured with the two capacitive probes.

The probes were mounted on a fixture which is hydraulically actuated into the steady-state plasma for no more than 1/2 second. The travel of the probes was adjusted so that both capacitive probe no. 1 and the Langmuir probe were positioned 7 cm from the plasma axis

in the equatorial plane of the torus, midway between two coils, when data were being taken. Capacitive probe no. 1 and the Langmuir probe were displaced axially 1 cm from each other. This arrangement allows us to measure the density and potential fluctuations at the same minor radius in the plasma, without reference to the axial dimension in the case of waves whose axial wavelength, $\lambda_{||}$, is much larger than 1 cm. Capacitive probe no. 2 was located 30° above the equatorial plane, in the same vertical plane and at the same plasma radius as the Langmuir probe. The probe array was inserted into a sector which did not contain an electrode.

As indicated schematically in Fig. 1, the signals from all three probes are digitized, and transferred to a computer where their respective Fourier transforms are computed. From the Fourier transforms we compute a variety of spectra to be described in the next section. At this point we wish to emphasize that the azimuthal wave number $k_\theta(\omega)$ can be determined from the phase of the cross-power spectrum between the two potential probe signals by following the procedures outlined in (6,7). The quadrature spectrum $Q_{n\phi}(\omega)$ between density and potential fluctuations is computed from the Fourier transforms of $\tilde{n}(t)$ and $\tilde{\phi}_1(t)$ following the procedures outlined in (1). Eq. (3) is then used to compute the transport spectrum $T(\omega)$.

CHARACTERISTIC EXPERIMENTAL RESULTS

We now present examples of transport spectra, and other spectra of interest, that were obtained during a study of fluctuation-induced

transport on the NASA Lewis Bumpy Torus plasma. It is our purpose to offer these examples as "proof of the concept" originally described in (1). A detailed discussion of transport in this particular plasma is beyond the scope of this paper. Further information on this latter topic may be found in (5).

All the spectra shown in this paper were computed following the procedures described in (7). The spectra were computed from a time series consisting of 2048 8-bit samples taken every 1 μsec. Thus, the duration of each record is 2.048 ms, and the Nyquist frequency is 500 kHz. The plots were frequency averaged over m=9 elementary frequency bands, resulting in a spectral bandwidth (the frequency separation between the discrete points) of 4.39 kHz (= 9/2.048 ms). A cosine-bell data window was applied to the raw time series data in order to reduce the effects of leakage.

Although Eq. (3) indicates that one only need to compute $k(\omega)$ and $Q_{n\phi}(\omega)$ to get $T(\omega)$, Eq. (4) suggests that additional insight may be obtained from knowledge of $n_{rms}(\omega)$, $\phi_{rms}(\omega)$, $\alpha_{n\phi}(\omega)$ and $|\gamma_{n\phi}(\omega)|$. Thus, for each experimental run we generate 6 spectral plots which permit us to measure each of the six parameters mentioned in the preceding sentences. In addition, we plot the transport spectrum $T(\omega)$ and the cumulative transport spectrum, which is to be defined later.

To demonstrate the usefulness of the fluctuation-induced plasma transport diagnostic we have selected four experimental data runs, and present the relevant spectral plots for each run in Figs. 2-5, respectively.

Note that each figure consists of eight computer-generated spectra. The spectra labeled (a) through (f) correspond to the six spectral quantities that appear on the right hand side of Eqs. (3) and (4). Spectra (g) and (h) are plots of the transport spectrum and the cumulative transport spectrum.

Spectrum (a) is a plot of the auto-power spectrum of $\tilde{\phi}_1(t)$. All system calibration factors have been taken into account so that the ordinate of each data point corresponds to the mean square value (i.e., $\phi^2_{rms}(\omega)$) of the potential fluctuations over a spectral bandwidth of 4.39 kHz. Spectrum (b) is the auto-power spectrum of the density fluctuations (i.e., $n^2_{rms}(\omega)$).

Spectra (c) and (d) are both phase spectra. Spectrum (c) corresponds to the phase $\theta_{12}(\omega)$ of the cross-power spectrum computed from $\tilde{\phi}_1(t)$ and $\tilde{\phi}_2(t)$. From the phase spectrum $\theta_{12}(\omega)$, one can readily determine $k_\theta(\omega)$, in the fact the right-hand axis has been scaled directly in terms of $k_\theta(\omega)$ using the approach described in (6,7). Knowing $k_\theta(\omega)$ one can compute the azimuthal phase velocity $\omega/k_\theta(\omega)$. We note that, generally speaking, the phase velocities associated with the $k_\theta(\omega)$ plots in Figs. (2-c), (3-c), (4-c), and (5-c) are of the order of 10^6 cm/sec. We also note that this is within a factor of two of the E_rXB drift, where E_r(100V/cm) is the static radial electric field resulting from d.c. voltage applied to the electrode rings and B(0.67T) is the toroidal magnetic field at the point at which the measurements are being made.

Spectrum (d) is the phase of the cross-power spectrum computed from $\tilde{\phi}_1(t)$ and $\tilde{n}(t)$ and thus represents the phase difference $\alpha_{n\phi}(\omega)$ between the density and potential fluctuations on a spectral basis.

The quadrature spectrum $Q_{n\phi}(\omega)$ is plotted as spectrum (e) and is used along with $k_\theta(\omega)$ from spectrum (c) to compute the transport spectrum $T(\omega)$ from Eq. (3).

The square of the degree of mutual coherence $|\gamma_{n\phi}(\omega)|^2$ is plotted as spectrum (f). It enters into Eq. (4) because we are considering polychromatic fluctuations rather than the special case of monochromatic fluctuations where $|\gamma_{n\phi}| = 1$. Further properties of coherence spectra are discussed in (8).

The transport spectrum $T(\omega)$ is plotted as spectrum (g). Since the transport spectrum is computed from digitized data we actually plot a transport spectrum (no. particles/area-time) not a transport spectral density function (no particles/area-time-frequency). Thus the ordinate of each point in the transport spectrum denotes the fluctuation-induced transport associated with a spectral-band of width 4.39 kHz, centered at the point in question. The transport spectrum $T(\omega)$ is a real quantity and may take on either a positive or negative value indicating that the transport is in either the inward or outward direction, respectively. Note that Eq. (3) indicates that there are only two quantities which determine the sign of $T(\omega)$, and hence the direction of transport. The first quantity is the phase-difference $\alpha_{n\phi}(\omega)$ between density and potential fluctuations. If $\alpha_{n\phi}(\omega)$ changes sign, $T(\omega)$ changes sign, since $T(\omega)$ is proportional to $\sin [\alpha_{n\phi}(\omega)]$.

The second quantity determining the sign of $T(\omega)$ is the sign of $k_\theta(\omega)$, which in turn is determined by the direction of propagation (in the azimuthal direction) of the wave.

Spectrum (h), $CT(\omega)$, is the cumulative transport spectrum which is found by summing the transport spectrum $T(\omega)$ from zero frequency up to the frequency in question. The value of $CT(\omega)$ at 500 kHz denotes the total fluctuation-induced transport associated with the fluctuation spectrum extending from zero to 500 kHz.

All data presented in Figs. 2-5 were obtained with D-shaped electrode rings inserted into the midplane of two (of the twelve) adjacent toroidal sectors. The operating conditions under which the data wwere taken is listed at the top of each figure, where V_A denotes the bias voltage applied to each electrode ring, I_A the discharge current, p_o the neutral gas pressure, and $\bar{n}_e$ the average electron density as measured by a microwave interferometer. All measurements were taken in deuterium gas.

The crucial difference between Figs. 2 and 3 is that data in Fig. 2 were taken while the electrodes were biased negatively, whereas the data taken in Fig. 3 were obtained with the electrodes biased positively. In Fig. 2 the transport spectrum $T(\omega)$ and the cumulative transport spectrum $CT(\omega)$ is positive (corresponding to radially inward fluctuation-induced transport), whereas in Fig. 3 $T(\omega)$ and $CT(\omega)$ are for the most part negative, indicating radially outward transport. Examination of Figs. (2-d) and (3-d) indicates that the phase difference between density and potential fluctuations $\alpha_{n\phi}(\omega)$ is for

the most part negative in both cases and thus is not responsible for the reversal of the transport direction. However, comparison of Figs. (2-c) and (3-c) indicate that $k_\theta(\omega)$ has changed sign, which, according to both Eqs. (3) and (4), results in a change in the direction of the fluctuation-induced transport. We attribute the change in sign of $k_\theta(\omega)$ (which indicates a reversal in the direction of azimuthal propagation) as being due to a reversal of the static radial electric fields, resulting from the reversal of polarity of the bias voltage applied to the electrodes.

In the two runs represented by Figs. 4 and 5, the voltage applied to the electrode rings was the same in both magnitude and polarity. However, the strength of a weak vertical magnetic field was changed from 7.5 Gauss in Fig. 4 to 12.5 Gauss in Fig. 5. We note that in Fig. 4 $T(\omega)$ and $CT(\omega)$ are positive, whereas, in Fig. 5 they are negative. Comparison of Figs. (4-d) and 5-d), indicate that the reversal in the direction of transport is due to a reversal in the sign of the phase relations ($\alpha_{n\phi}(\omega)$) between the density and potential fluctuations.

DISCUSSION

Although probes were used to monitor density and potential fluctuations, the diagnostic technique described in this paper may be utilized in conjunction with other methods (e.g., heavy-ion beam probes) of measuring density and potential fluctuation data.

The digital spectral analysis techniques applied in the examples above are capable of: (1) providing a quantitative measure of the fluctuation-induced transport in absolute physical units, (2) indicating the spectral dependence of the transport, and (3) providing additional experimental insight into the factors affecting both the magnitude and direction of transport. For example, Figs. 2-5 indicate that the radial fluctuation-induced ion transport observed in the NASA Lewis Bumpy Torus plasma at the probe location may be radially inward or outward. Generally speaking, it is found that for negatively biased electrodes (and a suitably adjusted vertical magnetic field) the fluctuation induced ion transport is radially inward, except in those sectors containing the electrode rings, where the ion transport is outward. For positively biased electrodes, the ion flux reverses direction in both the empty sectors and those containing the electrode rings. This results in a lower overall steady-state plasma density (5).

The diagnostic technique described in this paper provides important experimental insight into the fluctuation-induced transport processes governing the plasma confinement in this particular Bumpy Torus experiment (5). We anticipate that it could also be used quite fruitfully in measurements of fluctuation-induced transport in other magnetic confinement experiments as well.

REFERENCES

[1] E. J. POWERS, "Spectral Techniques for Experimental Investigation of Plasma Diffusion Due to Polychromatic Fluctuations," Nucl. Fusion, vol. 14, 749-752, 1974.

[2] E. O. BRIGHAM, The Fast Fourier Transform, New Jersey: Prentice-Hall, 1974.

[3] J. R. ROTH and G. A. GERDIN, "Characteristics of the NASA Lewis Bumpy Torus Plasma Generated with High Positive or Negative Applied Potentials," Plasma Phys., vol. 19, 423-446, 1977.

[4] C. E. BOYD, J. Y. HONG, E. J. POWERS, W. M. KRAWCZONEK, and J. R. ROTH, "A Data Acquisition System Employing a Microcomputer as a Programmable Interface Between Digital Transient Recorders and a Digital Tape Deck," submitted for publication.

[5] J. R. ROTH, W. M. KRAWCZONEK, E. J. POWERS, J. Y. HONG, and Y. C. KIM, "Inward Transport of a Toroidally Confined Plasma Subject to Strong Radial Electric Fields," Phys. Rev. Lett., vol. 40, 1450-1453, May 29, 1977.

[6] D. E. SMITH and E. J. POWERS, "Experimental Determination of the Spectral Index of a Turbulent Plasma From Digitally Computed Power Spectra," Phys. Fluids, vol. 16, 1373-1374, 1973.

[7] D. E. SMITH, E. J. POWERS, and G. S. CALDWELL, "Fast-Fourier-Transform Spectral Analysis Techniques as a Plasma Fluctuation Diagnostic Tool," IEEE Trans. Plasma Sci., vol. PS-2, 261-272, 1974.

[8] Y. C. KIM and E. J. POWERS, "Effects of Frequency Averaging on Estimates of Plasma Wave Coherence Spectra," IEEE Trans. Plasma Sci., vol. PS-5, 31-40, 1977.

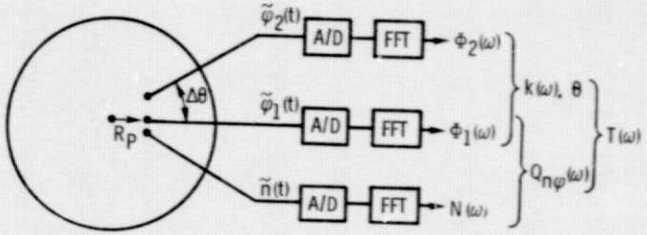

R_P = 7 cm, $\Delta\theta = 30^0$

$\tilde{\varphi}_1(t)$ measured with capacitive probe no. 1

$\tilde{\varphi}_2(t)$ measured with capacitive probe no. 2

$\tilde{n}(t)$ measured with Langmuir probe

Figure 1. - Schematic of the probe assembly and data acquisition system. The potential fluctuations are measured by capacitive probes; the ion density fluctuations by a Langmuir probe biased to ion saturation.

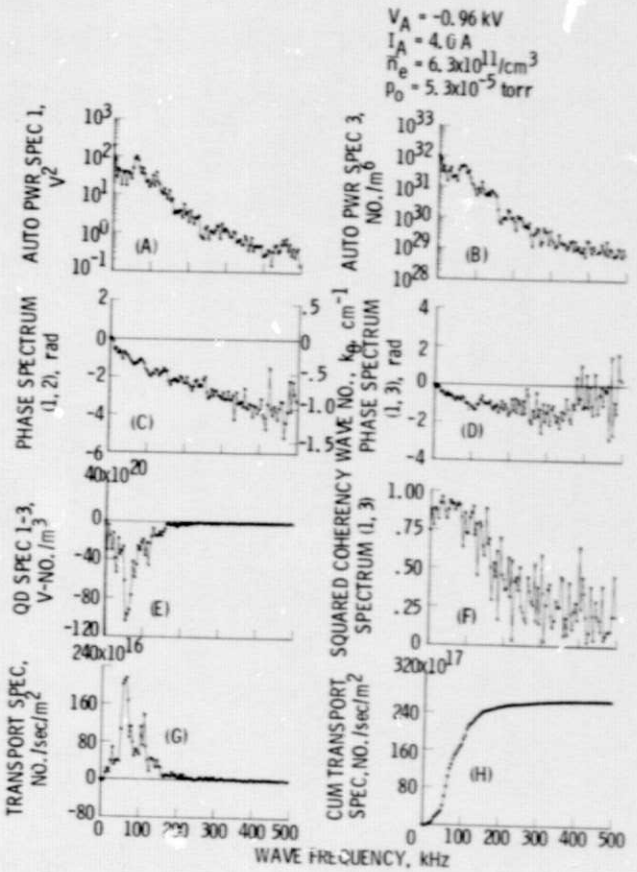

Figure 2. - Computer-generated fluctuation spectra or a confinement-optimized, negatively biased plasma with the radial electric field pointing inward.

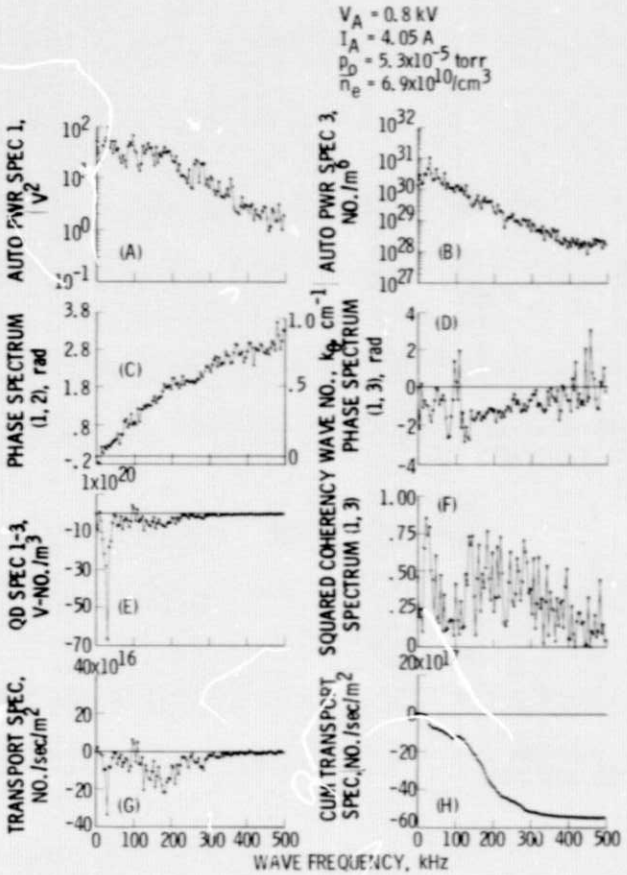

Figure 3. - Computer-generated fluctuation spectra for a confinement-optimized positively biased plasma with the radial electric field pointing outward.

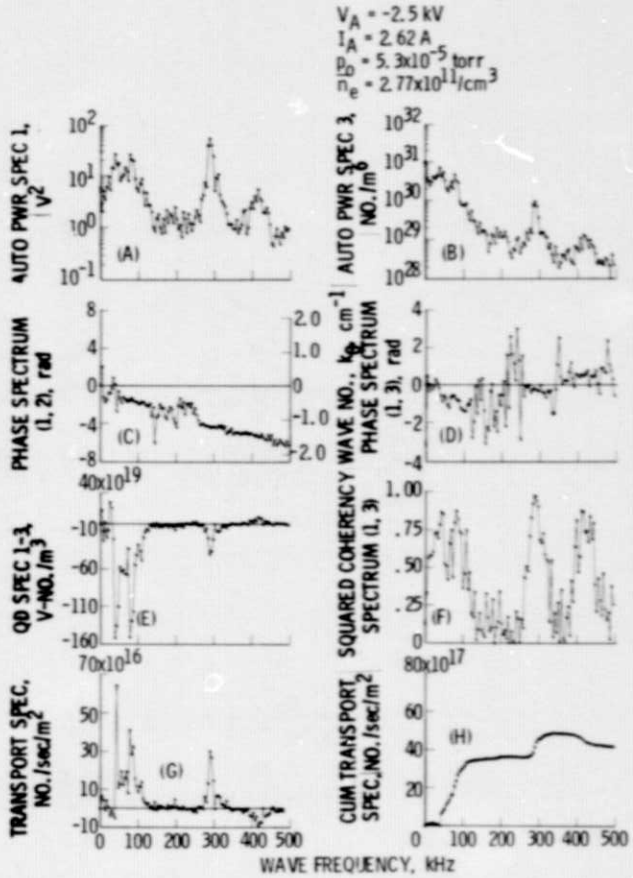

Figure 4. - Computer-generated fluctuation spectra for a plasma with the radial electric field pointing inward, and a weak vertical magnetic field of 7.5 gauss applied to the plasma containment volume.

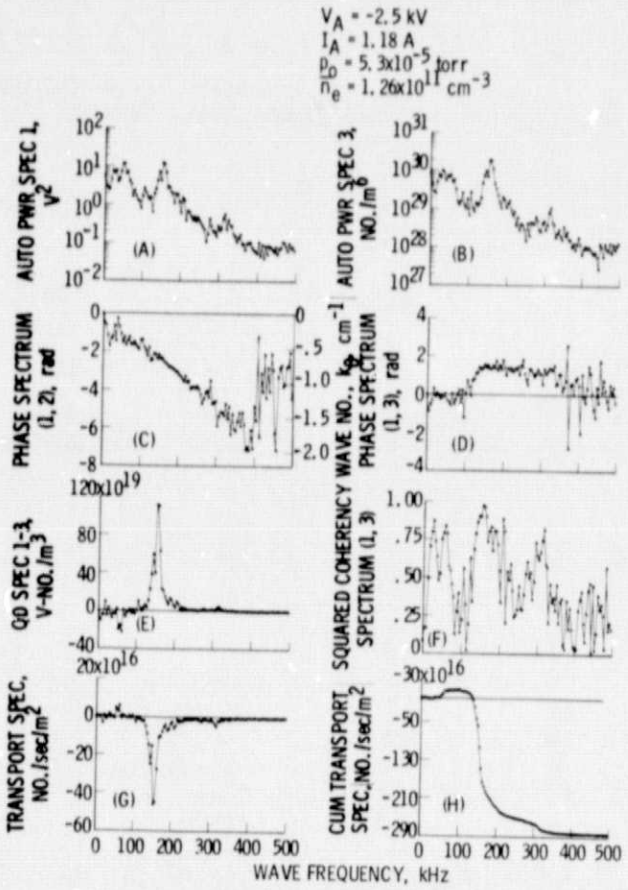

Figure 5. - Computer generated fluctuation spectra for same conditions as figure 4, but with a weak vertical field of 12.5 gauss.

1. Report No. NASA TM-78932	2. Government Accession No.	3. Recipient's Catalog No.
4. Title and Subtitle A FLUCTUATION-INDUCED PLASMA TRANSPORT DIAGNOSTIC BASED UPON FAST-FOURIER TRANSFORM SPECTRAL ANALYSIS		5. Report Date 6. Performing Organization Code
7. Author(s) E. J. Powers, Y. C. Kim, and J. Y. Hong, The University of Texas at Austin, Austin, Texas 78712; J. R. Roth and W. M. Krawczonek, Lewis Research Center, Cleveland, Ohio 44135		8. Performing Organization Report No. E-9675 10. Work Unit No.
9. Performing Organization Name and Address National Aeronautics and Space Administration Lewis Research Center Cleveland, Ohio 44135		11. Contract or Grant No. 13. Type of Report and Period Covered Technical Memorandum
12. Sponsoring Agency Name and Address National Aeronautics and Space Administration Washington, D.C. 20546		14. Sponsoring Agency Code
15. Supplementary Notes		

16. Abstract

The objective of this paper is to describe a diagnostic, based on fast Fourier-transform spectral analysis techniques, that provides experimental insight into the relationship between the experimentally observable spectral characteristics of the fluctuations and the fluctuation-induced plasma transport. The key ideas underlying the approach have been described elsewhere. In this paper, we review the model upon which the diagnostic technique is based, describe its experimental implementation, and present as examples some characteristic results obtained during the course of an experimental study of fluctuation-induced transport in the electric field dominated NASA Lewis Bumpy Torus plasma.

17. Key Words (Suggested by Author(s))	18. Distribution Statement
Plasma transport; Radial transport; Pedersen currents; Particle confinement; Fluctuation-induced transport; Plasma diagnostics	Unclassified - unlimited STAR Category 75

19. Security Classif. (of this report)	20. Security Classif. (of this page)	21. No. of Pages	22. Price*
Unclassified	Unclassified		

* For sale by the National Technical Information Service, Springfield, Virginia 22161